Supplementary Material

S1. Real HFR and ADCP observations data. Temporal cross-correlations with a confidence level of 99%. All the available data series of each dataset used. The results presented here complement the results shown in Rubio et al. (2019).

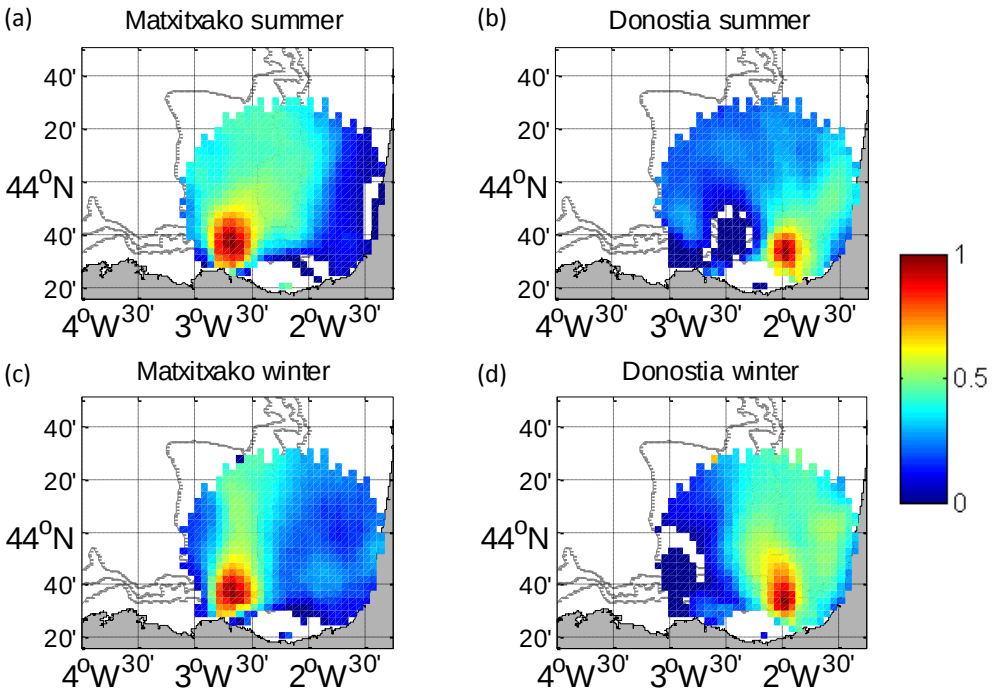

Figure S1. Temporal cross-correlation maps between the low-pass filtered time series of the HFR at Matxitxako (a, c) and Donostia (b, d) locations and the rest of the nodes within the HFR footprint area for V and for each season: summer (a, b) and winter (c, d). The results for the U component are shown in Rubio et al., 2019.

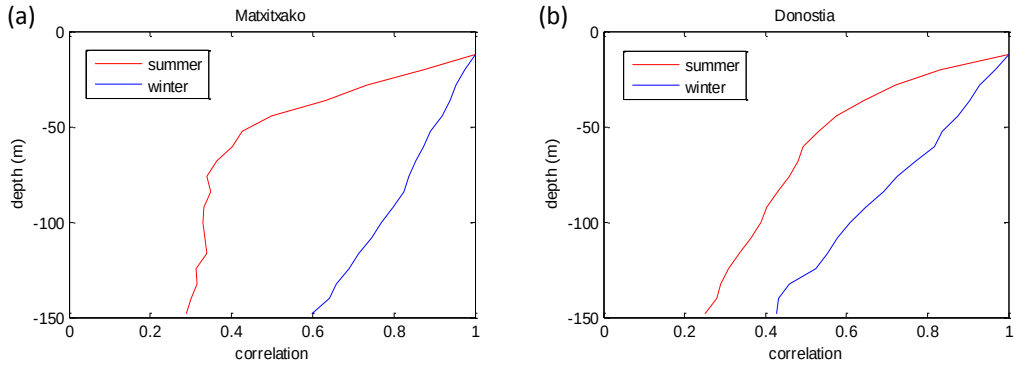

Figure S2. Low-pass filtered ADCP temporal V cross-correlations between the first bin (-12.26 m) and the rest of the bins along the water column for Matxitxako (a) and Donostia (b) for the summer (stratified) and winter (well-mixed) periods. The results for U are shown in Rubio et al., 2019.

5

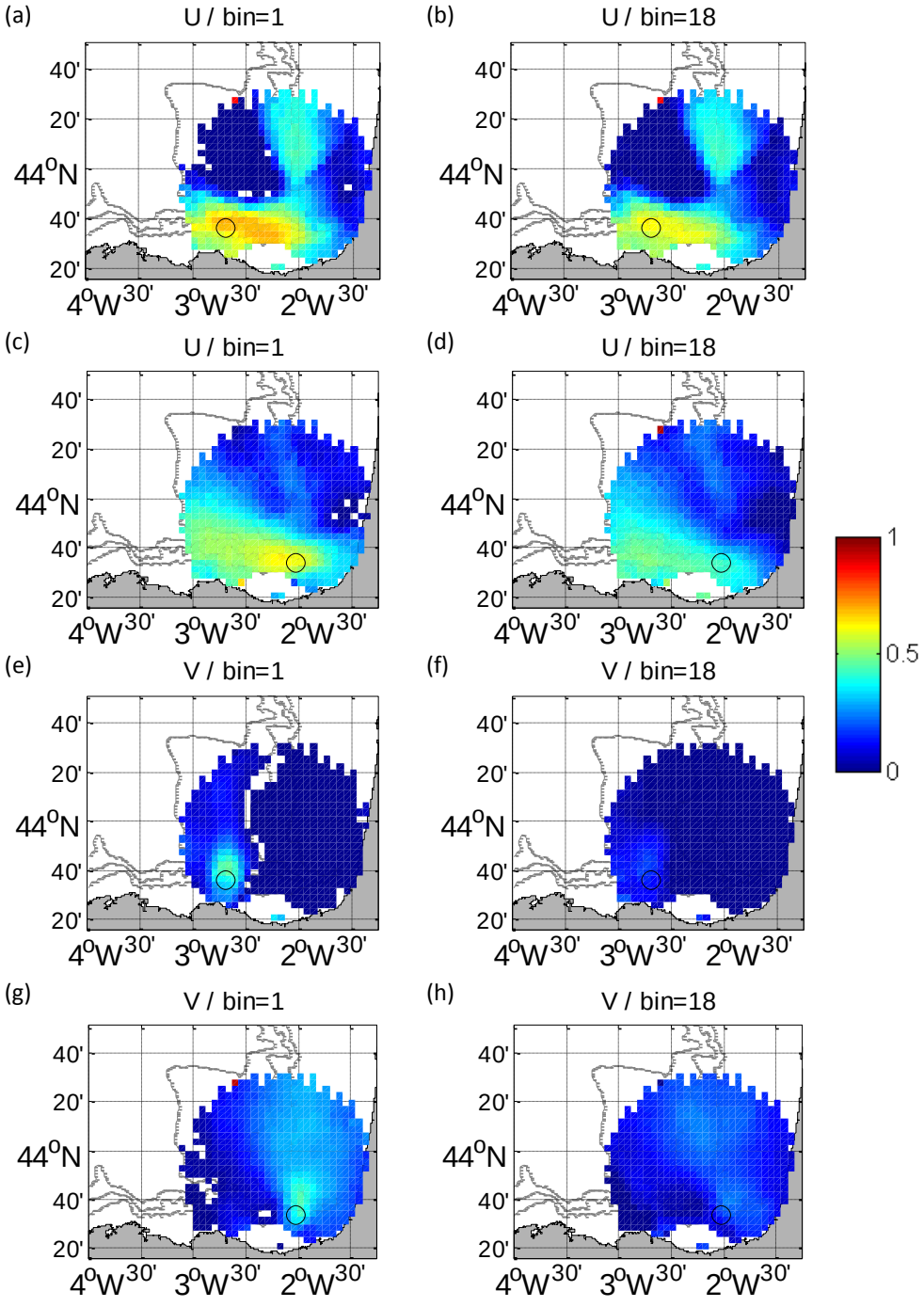

Figure S3. Temporal cross-correlation maps between the low-pass filtered time series of the HFR at the surface and the low-pass filtered ADCP time series for the bin 1 (-12.26m) (a, c, e, g) and 18 (-148.26m) (b, d, f, h) at Matxitxako (a, b, e, f) and at Donostia (c, d, g, h) and for U (a, b, c, d) and V (e, f, g, h). The black circles depict the positions of the ADCPs.

S2. RRMSD maps for ROOI with GLORYS-HR.

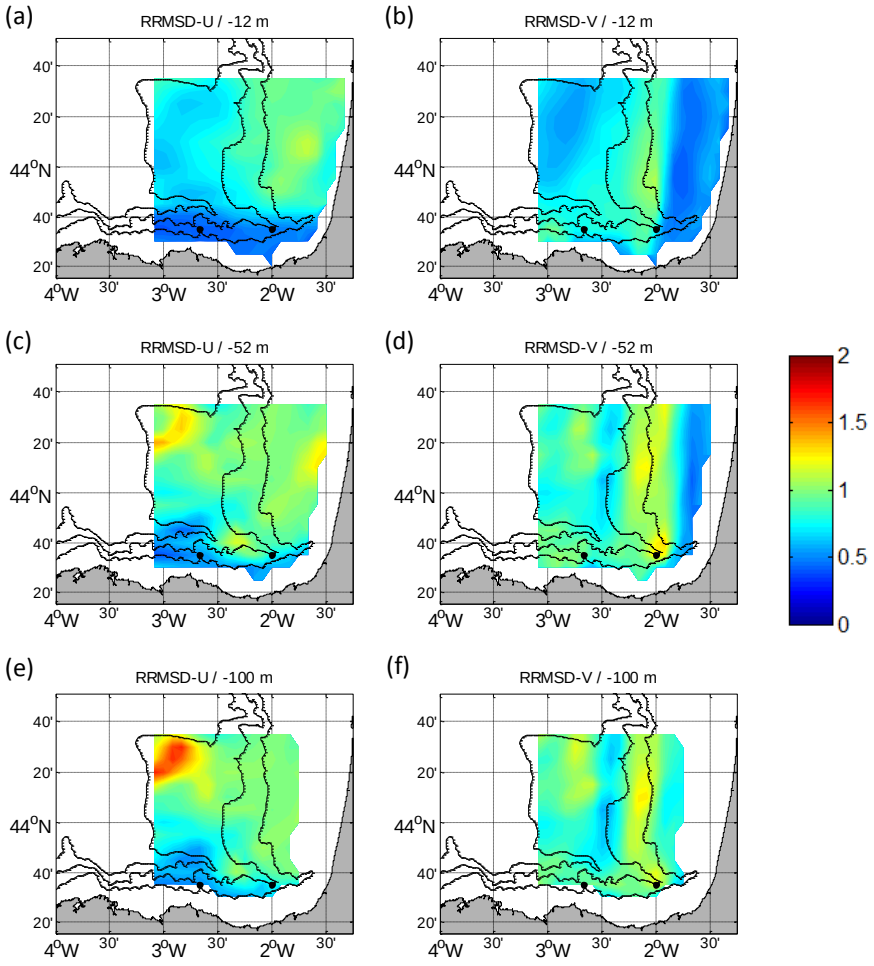

Figure S4. RRMSD maps for the summer period between the reference fields and the outputs of the ROOI with GLORYS-HR for U (a, c, e) and V (b, d, f). Different depths considered: -12 m (a, b), -52 m (c, d) and -100 m (e, f). The black dots depict the locations of the ADCPs.

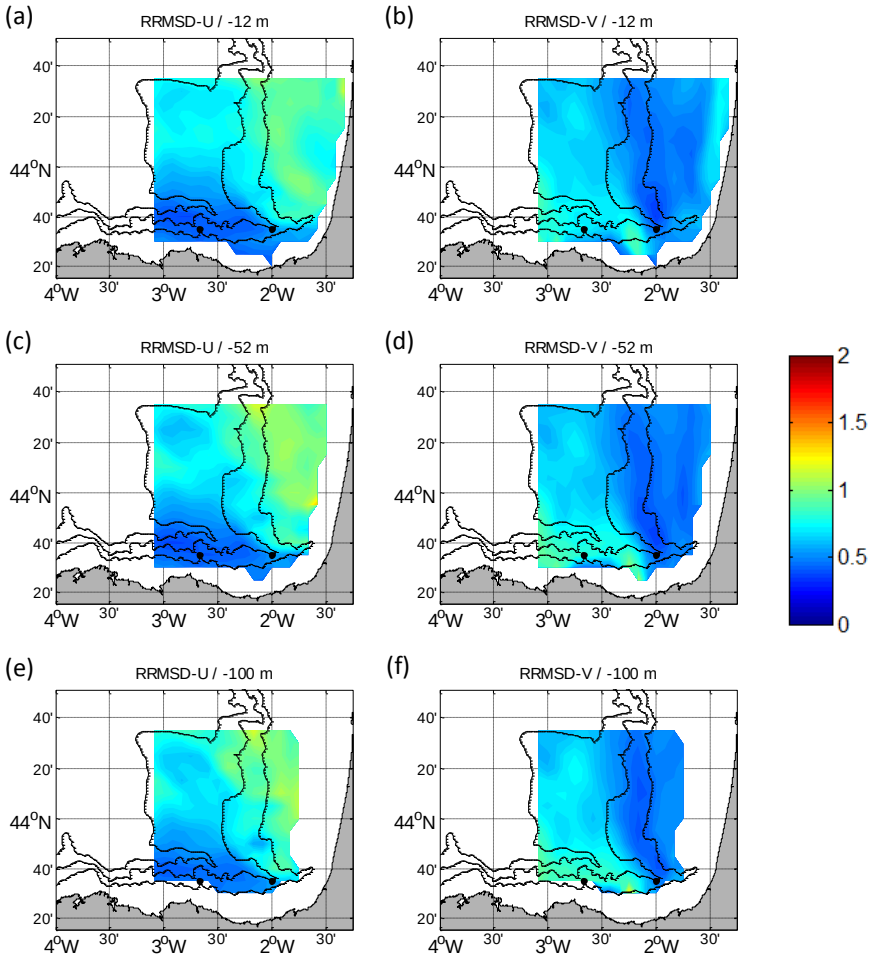

Figure S5. RRMSD maps for the winter period between the reference fields and the outputs of the ROOI with GLORYS-HR for U (a, c, e) and V (b, d, f). Different depths considered: -12 m (a, b), -52 m (c, d) and -100 m (e, f). The black dots depict the locations of the ADCPs.

5

S3. DCT-PLS RRMSD-U maps with higher colorbar values.

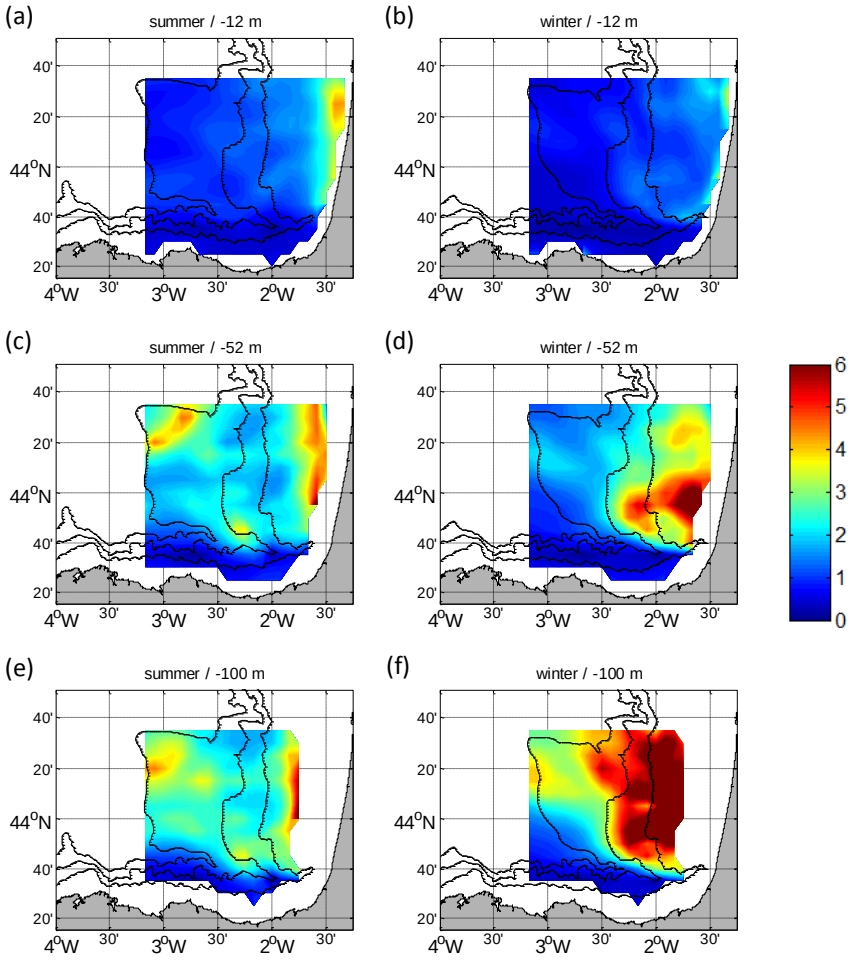

Figure S6. RRMSD-U maps for DCT-PLS for the summer period (a, c, e) and for the winter period (b, d, f).

S4. RMSD maps and spatial mean RMSD graphs.

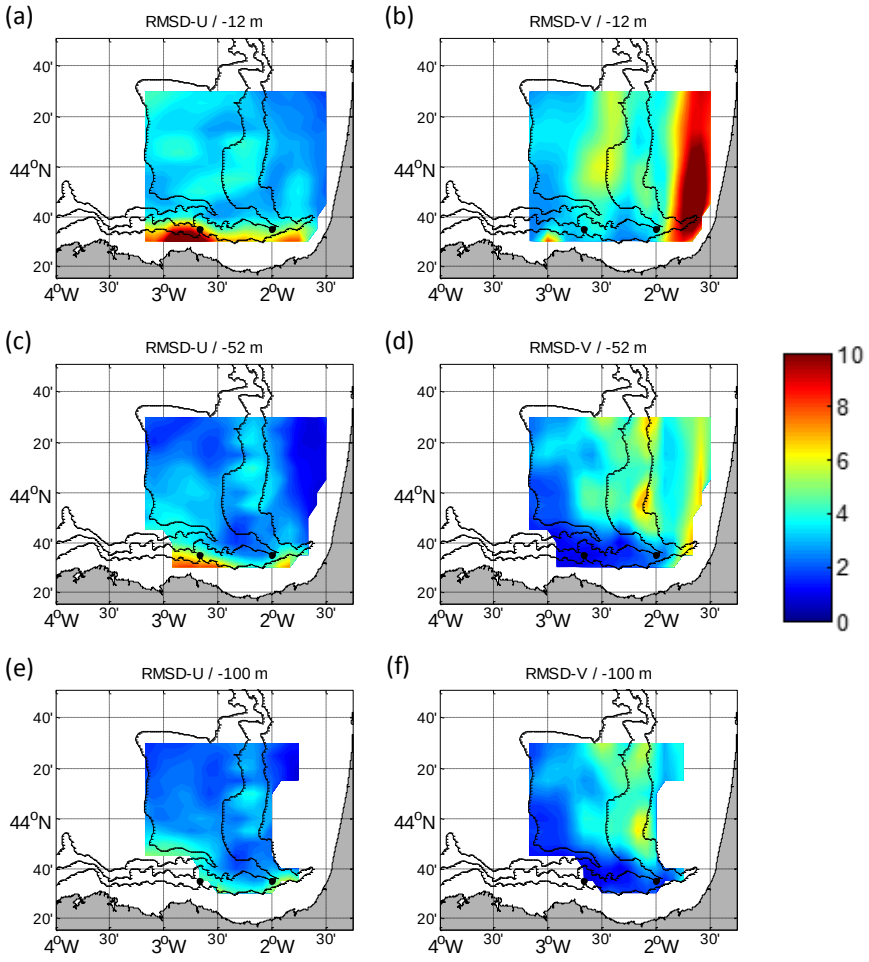

Figure S7. RMSD maps for the summer period between the reference fields and the outputs of the ROOI with GLORYS-LR for U (a, c, e) and V (b, d, f). Different depths considered: -12 m (a, b), -52 m (c, d) and -100 m (e, f). The black dots depict the locations of the ADCPs.

5

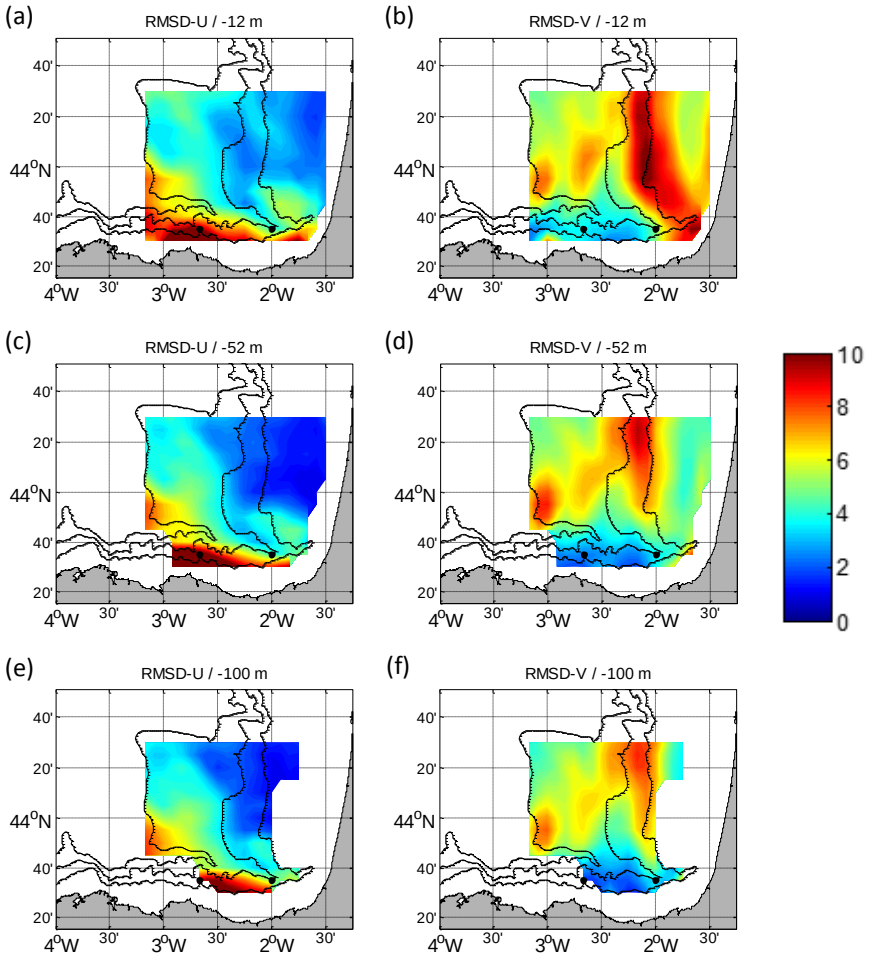

Figure S8. RMSD maps for the winter period between the reference fields and the outputs of the ROOI with GLORYS-LR for U (a, c, e) and V (b, d, f). Different depths considered: -12 m (a, b), -52 m (c, d) and -100 m (e, f). The black dots depict the locations of the ADCPs.

5

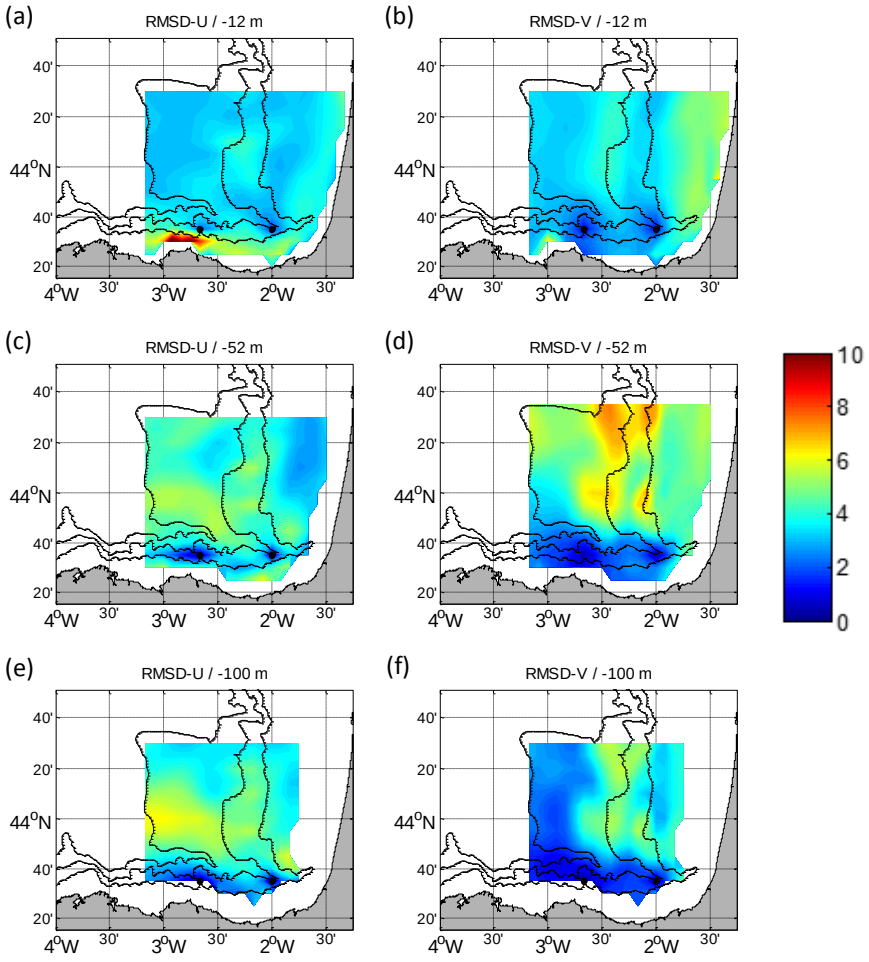

Figure S9. RMSD maps for the summer period between the reference fields and the outputs of the DCT-PLS for U (a, c, e) and V (b, d, f). Different depths considered: -12 m (a, b), -52 m (c, d) and -100 m (e, f). The black dots depict the locations of the ADCPs.

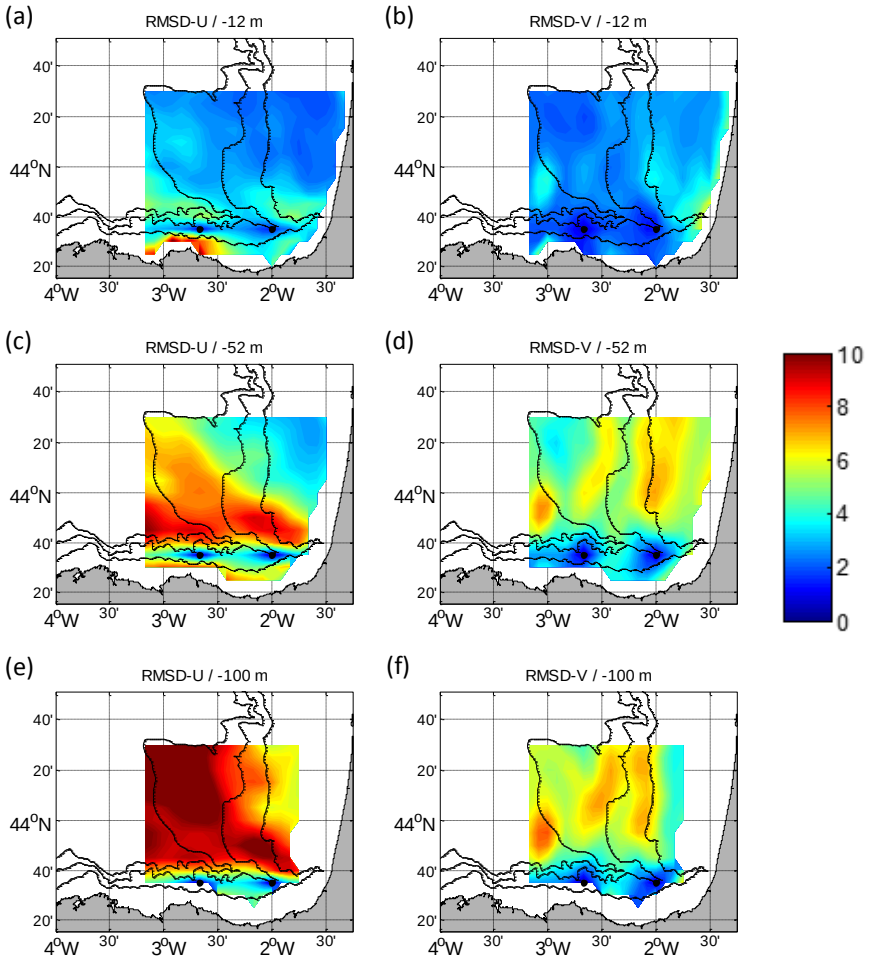

Figure S10. RMSD maps for the winter period between the reference fields and the outputs of the DCT-PLS for U (a, c, e) and V (b, d, f). Different depths considered: -12 m (a, b), -52 m (c, d) and -100 m (e, f). The black dots depict the locations of the ADCPs.

5

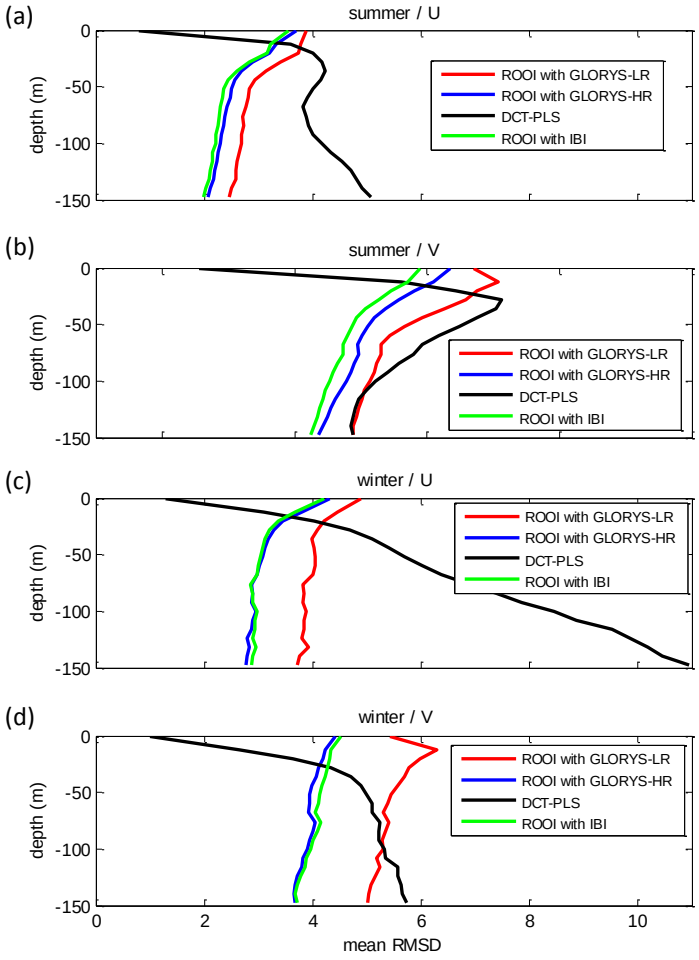

Figure S11. Mean RMSDs related to all the data-reconstruction methods for each depth considering the whole grid. For the summer period (a, b) and for the winter period (c, d). U in a, c and V in b, d.

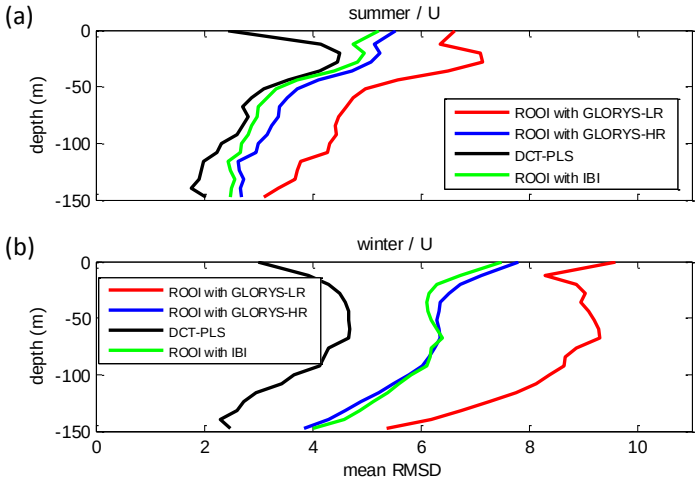

Figure S12. Mean RMSD-U related to all the data-reconstruction methods for each depth considering the reduced grid domain. For the summer period (a) and for the winter period (b).